Investigation of the effects of ion and water interaction on structure and chemistry of silicalite MFI type zeolite for its potential use as a seawater desalination membrane†

Bo Zhu,*[a] Linda Zou,[b] Cara M. Doherty,[c] Anita J. Hill,[c] Y. S. Lin,[d] Xiurong Hu,[e] Huanting Wang[f] and Mikel Duke[a]

Received 16th December 2009, Accepted 25th March 2010
First published as an Advance Article on the web 26th April 2010
DOI: 10.1039/b926455h

In this work we study the structural response of silicalite based MFI type zeolite powder to the presence of water and cations commonly found in sea salts including Na^+, K^+, Ca^{2+}, and Mg^{2+}. MFI zeolite powder was exposed to different solutions (3.8 wt% TDS (total dissolved solids) seawater (SW), or 1 M NaCl, or 0.05 M KCl), and their effects on the structure of the zeolite powder were characterized. The results obtained from ion adsorption testing and synchrotron X-ray powder diffraction showed that the zeolite powder interacted with water, monovalent and divalent cations, and these interactions altered the crystal dimensions of the zeolite. Most exposures to ions and water led to increases in crystal volumes of <0.1%, but exposure to KCl solution was observed to make the biggest contribution to crystal expansion, at 0.59%, particularly in the a- and c-directions as determined by Rietveld refinement. Upon closer inspection of SW exposed silicalite, a rapid exchange of Na^+ and K^+ was observed within 1 h, but after 8 h, these monovalent cations were gradually exchanged with divalent ions. Ca^{2+} was especially observed to adsorb into the zeolite at 8 h. N_2 adsorption and positron annihilation lifetime spectroscopy (PALS) measurements were made on SW exposed zeolites. PALS showed that the silicalite powder has mesopores (2.6 nm) and micropores (1.0 nm), which are both attributed to intercrystalline spaces. The intrinsic intracrystalline zeolite pore size was measured as 0.33 nm. Both N_2 adsorption and PALS showed that the relative amount of micropores to total pores decreased with seawater exposure which was attributed to ion adsorption and ion exchange. The mesopore size and number increase due to exposure, and although mesopores represent defects in crystalline zeolites, their expansion on exposure to seawater is important for membrane stability and diffusion properties and warrants further investigation. The intrinsic zeolite pore size was smaller in zeolites exposed to seawater (~0.29 nm), and the changes observed by PALS lead us to conclude that most of the ion activity observed is attributed to the intercrystalline micropores and mesopores. No other changes were observable by Fourier transform infrared spectroscopy (FTIR) and scanning electron microscopy (SEM) due to SW exposure. Results indicate that the interaction between silicalite and the water and ions in SW causes a change in structure and porosity expected to affect diffusion properties of these materials when used as membranes for desalination.

Introduction

Significant progress in the preparation and characterization of zeolite membranes has stimulated research in their application for various molecular level separations including gas phase and liquid phase mixtures. There has been some work to date applying zeolite membranes in the application of desalination, but there has been no work which explores how the dynamic polycrystalline lattice and grain boundaries interact with the water and ions to influence ion and water diffusion.

Zeolites are porous crystalline materials whose tuneable pore size, typically in the 0.3 to 1 nm range, makes them suitable for molecular sieving applications. Zeolites have been widely used in many scientific and technological fields due to their pore-related capabilities of ion exchange, adsorption, and catalysis. Their applications include air component separation, paraffin hydrocarbon separation and recovery, radioactive waste treatment,

[a]*Institute for Sustainability and Innovation, Victoria University, Werribee Campus, PO Box 14428, Melbourne, VIC, 8001, Australia. E-mail: bo.zhu@vu.edu.au; Fax: +61 3 9919 7696; Tel: +61 3 9919 8281*
[b]*Centre for Water Management & Reuse, University of South Australia, Mawson Lakes Campus, Adelaide, SA, 5095, Australia*
[c]*Materials Science and Engineering, The Commonwealth Scientific and Industrial Research Organization (CSIRO), Private Bag 33, Clayton South, VIC, 3169, Australia*
[d]*Department of Chemical and Materials Engineering, Arizona State University, Tempe, AZ, 85287, USA*
[e]*Center of Analysis and Measurement, Zhejiang University, Hangzhou, Zhejiang, 310058, P. R. China*
[f]*Department of Chemical Engineering, Monash University, Clayton, VIC, 3800, Australia*

† This paper is part of a *Journal of Materials Chemistry* themed issue on advanced materials in water treatments. Guest editors: Dongyuan Zhao, Benjamin S. Hsiao and Mietek Jaroniec.

hydrocarbon catalytic reactions, and air pollutant removal, *etc.*[1] Over the last decade, supported zeolite layers have been studied extensively for many potential applications such as separation membranes, catalytic membrane reactors, chemical sensors, *etc.*[2] Zeolite membranes rely on well-defined pores at the molecular level as well as the thermal, chemical, and mechanical stability of ceramics.[3] The studies of zeolite membranes have been mainly focussed on gas separation and liquid pervaporation processes. Molecular sieving and competitive adsorption and diffusion are the general separation mechanisms involved in zeolite membranes for these processes.[4–6]

Zeolites have also been shown to be outstanding candidate materials for desalination membranes as they possess the required small pore properties to reject ions.[7,8] As membranes, zeolites offer a chemically robust desalination option to desalinate 'challenging' waters present in the mining industry, or even reduce the cost of current desalination by reducing the replacement and cleaning costs of current polymer membrane technology. A molecular dynamic simulation study[8] showed that 100% rejection of Na^+ could be achieved using a perfect (single crystal), pure-silica ZK-4 zeolite membrane by reverse osmosis (RO). The size exclusion of hydrated ions is the separation mechanism of the perfect ZK-4 zeolite membrane. The aperture of the ZK-4 zeolite (diameter 0.42 nm) is significantly smaller than the kinetic sizes of hydrated ions.[9] Following this computational simulation study, several research groups have explored the possibility of using MFI-type zeolite membranes for desalination.[7,10–13] The MFI-type zeolite has orthorhombic crystal symmetry with nearly cylindrical, 10-member ring channels. The aperture size of the MFI-type zeolite is around 0.56 nm,[11] which is smaller than the sizes of hydrated ions. Performance testing of MFI type zeolite membranes working in reverse osmosis demonstrated that high rejections of even the smallest ions, including Na^+, are achievable.[7,12]

In general, permeation in an ideal molecular sieve zeolite membrane should occur only through the regular intracrystalline pores of the zeolite top layer. In reality, however, the permeation properties will often be modified due to the existence of intercrystalline defect porosity caused by insufficient intergrowth of crystals, thermal removal of the template, or the complete de-watering of the membrane layer.[14,15] In the synthesis of MFI type zeolites, tetra-propyl ammonium hydroxide (TPAOH) is usually used as a structure directing agent. Thermal removal of TPAOH has been extensively studied.[16,17] Several researchers have reported changes in the unit cell dimension of MFI type zeolite crystals during heat treatment.[15,18–20] In addition to the removal of the template and water, the adsorption of guest molecules such as benzene and n-hexane can also cause changes in the structure of zeolites.[21–23] However, little work has been carried out to explore the influence of seawater exposure and ion exchange on the intrinsic lattice dimensions and the intracrystalline and intercrystalline porosity of MFI zeolite. In this work, we expose the MFI framework zeolite (silicalite) to SW salts and explore the relative uptake of cations. We utilize synchrotron X-ray powder diffraction (the Australian Synchrotron) to measure the lattice changes associated with seawater exposure. We also utilize N_2 adsorption, positron annihilation spectroscopy (PALS), and FTIR to develop a better understanding of the effect of SW exposure on the structure of silicalite powder. This is the first reported evidence of the effect of water and ions in SW solution on the lattice structure, intracrystalline porosity, and intercrystalline porosity of silicalite. This work forms part of our ongoing research to develop tailored zeolite materials for desalination membranes and discover new desalination concepts from studies of molecular level structure property relationships.

Experimental

Material preparation

The silicalite MFI zeolite powder used for this study was prepared by calcining the suspension synthesized using a standard hydrothermal process[12] at 525 °C for 6 h with a temperature increase/decrease rate of 1 °C/min. The silicalite suspension was prepared from a solution of 43 mL of 1M TPAOH (Aldrich), 0.6 g NaOH (Aldrich) and 8.5 g fumed silica (Aldrich, particle size 0.014 μm, surface area 200 ± 25 m^2 g^{-1}) which was hydrothermally treated in a Teflon lined stainless steel autoclave at 180 °C for 8 h. The hydrothermal synthesized suspension was thoroughly washed with deionized water (DIW) by repeating centrifugation and redispersion in DIW three times prior to the calcination.

Ion adsorption testing

The ion adsorption experiments were carried out in a shaking waterbath at room temperature. For each ion adsorption experiment, 1 g MFI zeolite powder was mixed with 5 mL solution (3.8 wt% (TDS) SW, or 1 M NaCl, or 0.05 M KCl) in a 50 mL centrifuge tube and shaken for a fixed time. The SW solution used in this work was prepared from sea salts (Sigma-Aldrich) containing a wide range of ions in varying amounts, with the most significant cations shown in Table 1 as measured in our laboratory. After each adsorption experiment, the mixture was centrifuged immediately to avoid any further interactions, and the solution sample was withdrawn from the tube and analyzed for cations by inductively coupled plasma-optical emission spectroscopy (ICP-OES). Cation analysis was performed using a Shimadzu ICPE-9000 ICP-OES. Ion adsorption testing was also conducted on the silicalite powder exposed only to DIW for comparison.

Table 1 Concentration of significant ions when made to 3.8 wt% (TDS) in water

Component	3.8 wt% (TDS) SW (mg L^{-1})
Sodium[a]	9885
Magnesium[a]	1185
Potassium[a]	346
Calcium[a]	361
Strontium[a]	13
Sulfate	2660
Chloride	19290
Boron	5.6
Bromide	56

[a] Ions measured in our laboratory.

Material characterization (SEM, FTIR, N_2 adsorption, PALS and powder diffraction)

The original and SW treated zeolite powders were characterized by SEM, FTIR, N_2 adsorption, PALS and synchrotron X-ray powder diffraction. SEM micrographs of MFI zeolites were taken for investigation of the particle morphology using a JEOL JSM–6300F scanning electron microscope (15 kV). The energy dispersive X-ray spectrometer (EDXS) attached to the SEM was used to conduct elemental analysis of the samples. A Shimadzu FTIR–8400S spectrometer (Shimadzu, Japan) with source setting 1200 W RF power was used for recording the FTIR spectra of the zeolite samples in the form of KBr pellets. IR spectra of the powder samples were recorded at 20 cm^{-1} spectral resolution. The number of scans was set at 12 and the regular scanning range used for the samples was 400–4000 cm^{-1}. N_2 adsorption experiments were carried out using a Tri Star 3000 porosity analyzer (Micromeritics, USA) at liquid N_2 temperature on samples degassed for 4 h at 150 °C. PALS experiments were performed using an automated EG&G Ortec fast-fast coincidence system with fast plastic scintillators and a resolution function of 230 ps FWHM. To measure the long lifetimes, the range of the time-to-amplitude converter (TAC) was extended to 200 ns. The coincidence unit was removed due to the low count rates. The 50 μCi ^{22}NaCl source was dried onto 2.54 μm thick Ti foil which required no background subtraction. The samples were degassed at 150 °C under vacuum for 16 h prior to measurement. The foil source was sandwiched between 2 mm of sample and evacuated to 5×10^{-7} Torr. A minimum of five spectra of 4.5 million integrated counts were collected per sample. The spectra were analyzed using LT9 and were fitted to five components with τ_1 being fixed to 0.125 ns due to para-positron self-annihilation, and $\tau_2 \sim 0.35$–0.45 ns attributed to free positron annihilation. The average pore diameter for τ_3 was calculated using the Tao–Eldrup model assuming infinitely long cylindrical pore shape.[24,25] The pore sizes for the long lifetimes (τ_4 and τ_5) were calculated using the rectangular Tao–Eldrup (RTE) model based on an infinitely long channel.[26] Three commercial Type-A molecular sieves were analyzed under the same conditions to verify their intrinsic intracrystalline zeolite pore dimensions. Molecular sieves 3A, 4A (Sigma Aldrich) and 5A (BDH) were activated at 250 °C, ground and then measured under vacuum. Their intrinsic pores were found to be 0.302, 0.294 and 0.352 nm respectively using the Tao–Eldrup model. Synchrotron X-ray powder diffraction measurements were conducted at the Australian Synchrotron to measure the crystalline structure of the zeolites initially and after SW exposure. Samples were placed in the sample cell and spun at 100 rpm to improve particle statistics in these polycrystalline sample measurements ensuring optimal peak intensity and symmetry. All the structure refinements were performed using the Rietveld method with MDI Jade 9.0 software (Materials Data Inc., USA). Further experimental and refinement details are shown in Table 2.

Table 2 Experimental and selected crystallographic parameters for MFI zeolites

Chemical formula	$\lvert Na^+_n(H_2O)_{16}\rvert[Al_nSi_{96-n}O_{192}]$-MFI ($n < 27$)[29]
Space group	Pnma
Powder diffractometer	Bending magnet beamline with Si (111) flat crystal monochromator
Beam energy (KeV)	12.3984
2-theta range (°)	3.193645–82.82114
Wavelength (Å)	1.0
Step size (2θ°)	0.00375
Counting time (s)	1
Acquisition time (s)	120
No. of data points	21235

Results and discussion

Ion adsorption

To better understand the interaction of ions and water with silicalite, studies of ion interactions between silicalite powder and various solutions were carried out. Cation exchange by the zeolite was measured using ICP-OES. Table 3 lists the elemental concentrations obtained from ICP-OES for major cations present in the original and silicalite treated solutions. The adsorption results for DIW are also included in Table 3 for comparison.

It can be seen that silicalite interacted with each solution during the 64 h exposure. DIW caused a release of Na^+ from the lattice most likely due to ion exchange and the presence of residual Na^+ from sample preparation as NaOH was added in the synthesis solution. A release of K^+ into the DIW was also observed due presumably to hydrolysis. DIW, NaCl and SW ion adsorption results also showed a release of K^+ from the silicalite powder. The source of K^+ from the silicalite powder was investigated. ICP-OES analysis showed that the TPAOH solution, which was used as a structure directing agent in the synthesis of MFI type zeolites, contains a high level of potassium (around 2300 mg/L). This indicates that the potassium ions present as impurities in TPAOH are the source that caused the unusual increase of K^+ in the solutions treated by silicalite powders. It is common in zeolite synthesis that Na^+ and K^+ impurities come from the commercially available TPAOH solutions.[27] K^+ will exchange with Na^+ in silicalite as clearly shown by the KCl ion adsorption experiment (Table 3).

The silicalite treated SW showed a significant reduction in divalent ions Ca^{2+} (44.3%), Mg^{2+} (24.7%) and Sr^{2+} (46.1%), and increases in Na^+ (6.6%) and K^+ (61%). The increase in Na^+ and K^+ may be due to exchange with the divalent ions Ca^{2+}, Mg^{2+} and Sr^{2+}. The silicalite treated in NaCl solution should not undergo any exchange other than hydrolysis; however, the observed decrease in Na^+ and increase in K^+ are most likely due to Na^+ from solution exchanging with K^+ from the silicalite. For KCl solution, there was a 24% reduction in K^+ and the concentration of Na^+ increased from around 0 to 1564 mg L^{-1} after 64 h treatment with silicalite. As mentioned above, this result suggests that K^+ is preferentially taken into the zeolite and exchanged with Na^+. There were almost no changes in trace levels of Ca^{2+} between the original and silicalite treated solutions for both NaCl and KCl.

Ion interaction experiments were also conducted on the silicalite powder at different exposure times in SW. Fig. 1 shows the variation of concentrations of the cations in solution obtained from ICP-OES for the silicalite treated SW samples with varying

Table 3 Elemental concentrations of the cations in the untreated and silicalite treated solutions[a]

Exposure	Treatment time (h)	Concentration (mg L^{-1})				
		Ca	K	Mg	Na	Sr
DIW	0	UD	UD	UD	UD	UD
	64	~0	113	UD	401	UD
KCl	0	14	826	UD	UD	UD
	64	15	626	UD	1564	UD
NaCl	0	10	30	UD	22900	UD
	64	10	729	UD	22400	UD
SW	0	361	346	1185	9885	13
	64	201	888	904	10538	7

[a] SW = 3.8 wt% (TDS); NaCl = 1 M; KCl = 0.05 M; UD = undetected.

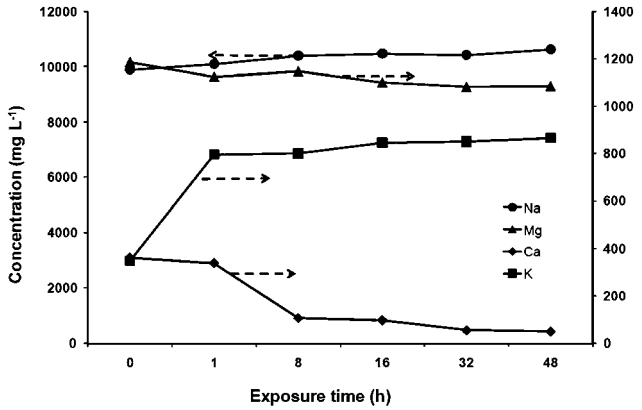

Fig. 1 Variation of concentrations of the cations in SW solution with exposure time.

exposure time. The concentrations of the divalent ions Ca^{2+} and Mg^{2+} decreased over the exposure time, with more significant reduction in Ca^{2+}, with most uptake occurring between 1 to 8 h exposure. Due to the small amount of Sr^{2+} in the SW solution the change in concentration as a function of time is not significant. Na^{+} in solution increases gradually with increasing treatment time, which is most likely due to exchange with the divalent ions. K^{+} in solution increases rapidly at 1 h and gradually thereafter.

SEM

SEM analysis was used to investigate the size and shape of the crystalline MFI particles. Fig. 2 shows the SEM micrograph of the original MFI silicalite powder sample. It can be seen that quite uniform cubic shaped MFI zeolite crystals were formed. The size of the crystals was found to be around 0.3 μm. No changes were observed in the particle morphology of the powder samples before and after exposure to SW. Elemental analysis of the silicalite powder samples was carried out by EDXS. Only Si and O were detected by EDXS analysis, with the O/Si ratios being around 4.2–4.8. None of the ions in seawater were observed by EDXS.

FTIR

The FTIR spectra of the original and treated silicalite powders are shown in Fig. 3. A number of distinct absorption bands (around 1100, 795, 545 and 450 cm^{-1}) resulting from the stretching and bending of the Si–O units in the zeolite framework are indicative of MFI type zeolites.[28] The absorption peak at 1100 cm^{-1} is assigned to the internal asymmetric stretching of the Si–O bonds, 795 cm^{-1} to the symmetric stretching of the Si–O bonds, 545 cm^{-1} to the pentasil double ring vibration, and 450 cm^{-1} to Si–O bending. The FTIR spectra show no significant differences before and after treatment in various solutions for 64 h.

Synchrotron X-ray powder diffraction

Synchrotron X-ray powder diffraction was used to determine changes in the crystalline structure of silicalite after ion adsorption. NIST LaB_6 standard SRM 660 was used as a reference material for the calibration of the wavelength and zero offset. Synchrotron X-ray powder diffraction measurements were repeated twice on selected powder samples, and the results showed a higher repeatability of the experiments. The synchrotron X-ray diffraction pattern taken at a wavelength of 1.0 Å for the as synthesized silicalite powder is shown in Fig. 4a. The silicalite sample with MFI type framework confirmed by X-ray diffraction (XRD) using CuKα radiation (wavelength = 1.54 Å) was also measured by synchrotron X-ray diffraction under the same environmental conditions for comparison. The powder samples treated by different solutions had the same MFI

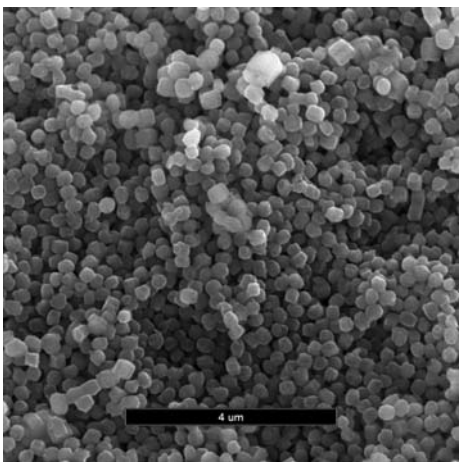

Fig. 2 SEM micrograph of the original MFI silicalite powder sample.

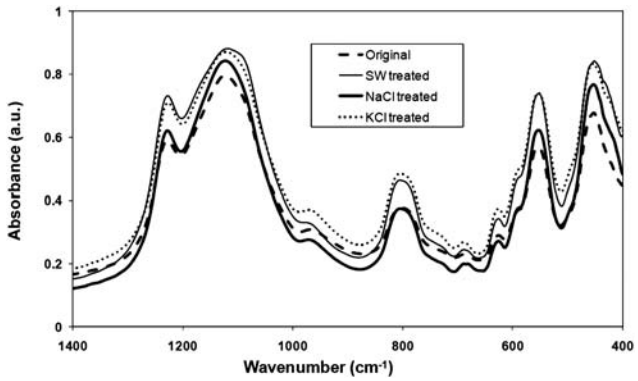

Fig. 3 FTIR spectra of the original and solution treated MFI silicalite powders.

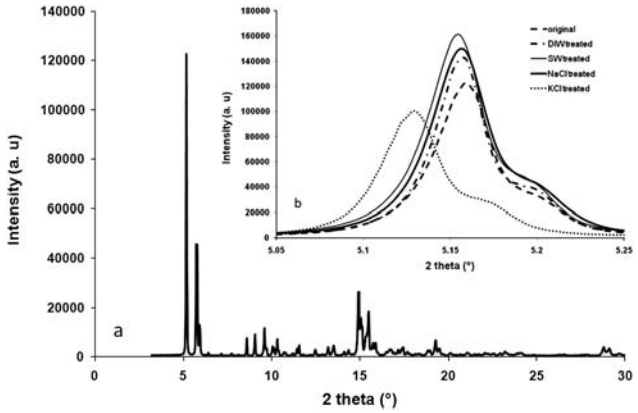

Fig. 4 Synchrotron X-ray powder diffraction pattern of a MFI type silicalite sample (a) and differences between the most intense Bragg peak for original and solution exposed silicalite samples (b).

fingerprint patterns (not shown here) to Fig. 4a but showed slight changes after exposure to different solutions for 64 h. These changes are highlighted in Fig. 4b inset.

To investigate the structure in three dimensions, structural refinement using the Rietveld method (Jade 9.0 software, MDI, USA) was carried out for original and 64 h exposed samples based on the X-ray synchrotron data. The fitting patterns of the original silicalite powder sample from Rietveld structural refinement are shown in Fig. 5 and the unit-cell parameters of the zeolite powder samples are given in Table 4. The lower trace in Fig. 5 shows the profile observed from the experiments, while the middle trace represents the calculated profile from the structure refinement. The difference between the calculated and observed profiles is shown as the upper trace in Fig. 5. It was found that

Table 4 Unit-cell parameters (nm) and volume (nm^3) of the silicalite powders before and after exposure to seawater ions

Silicalite sample	a	b	c	V
Original	2.04131(5)	2.01944(6)	1.35841(5)	5.5998
SW (64 h)	2.04264(6)	2.02065(6)	1.35934(5)	5.6106
NaCl (64 h)	2.04253(5)	2.02011(6)	1.35916(4)	5.6081
KCl (64 h)	2.05344(5)	2.03066(6)	1.36643(5)	5.6978

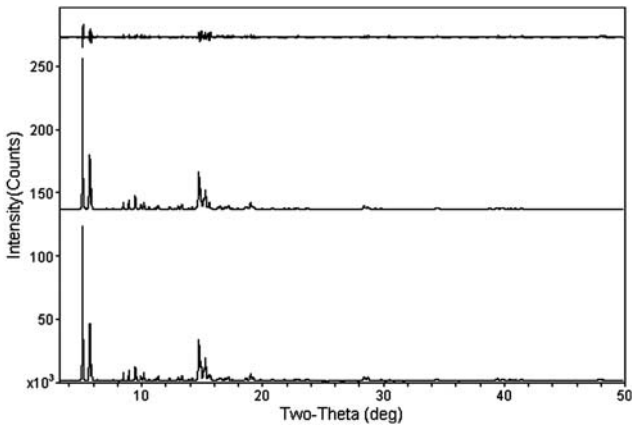

Fig. 5 Rietveld plots for the original silicalite powder: observed (lower trace), calculated (middle trace) and difference (upper trace) profiles.

the calculated and observed patterns fitted very well for the original silicalite powder. The Rietveld plots for the rest of the powder samples studied were similar to those of the original silicalite sample as shown in Fig. 5. Table 4 shows that the unit-cell parameters and volume of silicalite samples increased after 64 h exposure to different solutions compared to the original sample, especially for the powder treated by KCl solution. This result indicates that expansion occurs in the lattice structure of silicalite due to exposure of zeolite powders to different solutions.

By the Rietveld process, we can see that a slight overall expansion of the silicalite lattice was observed. Expansion along the a- and c-axis was more prominent for all the silicalite powder samples after 64 h exposure to different solutions (Fig. 6). Fig. 7 shows a schematic of the change in unit-cell dimensions (a-, b- and c) of silicalite crystals after exposure to seawater, with relatively more expansion in a- and c-directions as shown in Fig. 6. It is noticeable from Fig. 7 that the a- and c-directions are the dimensions for the largest pores along the [010] plane.[29] Positively charged ions in these pores, *e.g.* Na^+, K^+, balance the aluminium in the silicalite lattice; ionic radii of these cations are 0.093 nm and 0.133 nm, respectively. Although we have controlled conditions in our synthesis to exclude aluminium, our SSNMR measurements detected its presence which allows our zeolites to participate in ion exchange. We postulate that cations can expand the lattice dimensions as they enter the lattice or intercrystalline pore structure. The larger expansion of the KCl treated sample is most likely due to the preferential uptake of K^+ ions by the zeolite powder (Table 3). The key finding from this analysis is that K^+ will influence unit cell structure when in high enough concentration. For the SW samples which also contain K^+, the expansion is much lower compared to KCl exposed samples. Lattice expansions for silicalite MFI zeolite due to SW, NaCl, and pure water[15] exposure are similar (<0.1%).

N_2 adsorption and PALS results

The adsorption/desorption isotherms (not presented) of N_2 at 77 K for silicalite powders appeared to be a typical IV type[30] with a hysteresis loop that closes at a relative pressure p/p^0 of around 0.2. The samples are microporous in nature with a contribution from mesopores. The uptake of nitrogen at low relative pressures

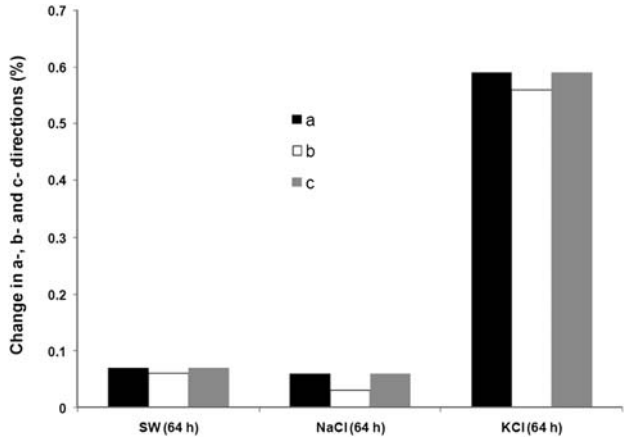

Fig. 6 Unit-cell dimension changes in a-, b- and c-directions after exposure to seawater ions.

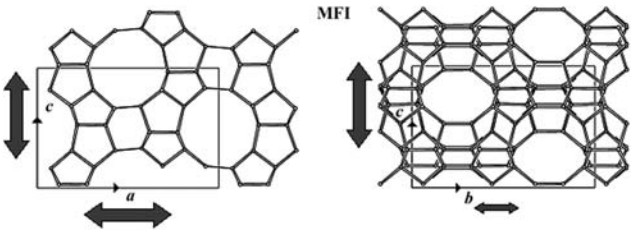

Fig. 7 Unit cell content in MFI projected along the b- (left) and a- (right) axes.[29] Arrows indicate relative expansion of the crystal measured in Fig. 6 due to uptake of ions or water.

($p/p^0 < 0.2$) is due to micropore filling.[31,32] The hysteresis loop at a relative pressure p/p^0 of around 0.2 is due to capillary condensation within mesopores.[33]

The adsorption isotherms of N_2 for the original and SW treated silicalite powders are compared in Fig. 8. Compared to the original sample, more N_2 was adsorbed after $p/p^0 = 0.2$ on all samples exposed to SW indicating an increase in the proportion of mesopores associated with this exposure.[34]

N_2 adsorption is limited by access of N_2 molecules into the structure. PALS does not rely on external accessibility of the pores and has been shown to characterize all spaces, even those

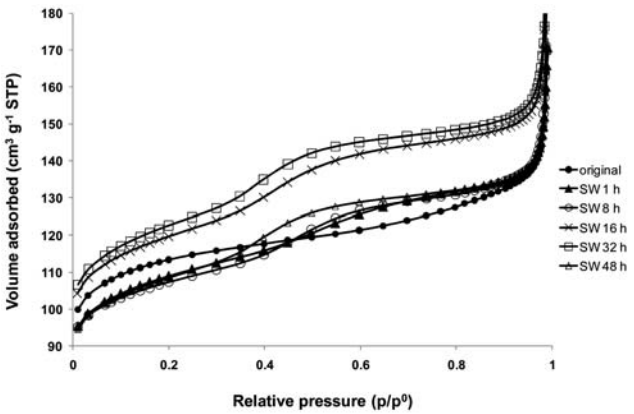

Fig. 8 Adsorption isotherms of N_2 for the original and SW treated silicalite powders at 77 K.

inaccessible to N_2, in H_2 selective molecular sieve silicas.[35] PALS has been used to study in situ and spin-on MFI zeolite films for use as low dielectric constant insulators in computer microprocessors.[36] Pure silica zeolite (PSZ) silicalite films prepared by in situ crystallization were shown to have a single uniform pore size of 0.55 nm, which correlates extremely well with the crystallographically determined pore size, whilst spin-on films of zeolite nanoparticle suspensions were shown to have the 0.55 nm intrinsic porosity as well as intercrystalline mesopores of size 2.6 nm.[36] Table 5 shows the results from PALS on the original and SW treated silicalite powders.

PALS measurements of porosity show that the silicalite powder contains mesopores (2.6 nm) and micropores (1.0 nm), and the zeolite lattice pore size is 0.33 nm (Table 5). The mesopore size is similar to that reported previously by PALS in PSZ silicalite[36] and by n-hexane porosimetry in silicalite-1 membranes.[37] Recently, the intracrystalline pores were measured by low pressure N_2 adsorption to be around 0.54 nm, but the same study also identified intercrystalline spaces of around 3–4 nm.[32] The 0.33 nm zeolite pore size is smaller than that previously reported for MFI zeolites by PALS (0.55 nm $\pm$ 0.03 nm),[36] by low pressure N_2 adsorption (0.54 nm)[32] or by crystallography (0.56 nm) for the 10-member ring openings.[11,29] This difference in pore size could be explained *via* two possible mechanisms. The first is that the positrons are accessing both the 0.55 nm pores and the smaller surrounding chambers within the MFI lattice. Therefore, 0.33 nm could be an average of the accessible intracrystalline spaces. The second explanation for smaller pore size measured with PALS is that the zeolites have sodium or potassium ions present within the pores, hence reducing the accessible pore diameter. The theoretical radius of 0.55 nm is determined for the pure aluminosilicate structure, and does not take into consideration the presence of cations.[1,38] Given that previously reported PALS results on pure silica zeolite (PSZ) silicalite films yield a single uniform pore size of 0.55 nm,[36] the latter explanation is most likely.

An intermediate lifetime of 7–8 ns with intensity of 3–4% was reported by Li *et al.*[36] for pure silica MFI zeolite thin films but was not attributed to micropores. As shown in Table 5 we measure an 8 ns lifetime with intensity of 18.2% in our original silicalite powder and attribute this to micropores of size 1.05 nm. Micropores of size between 1 nm and 2.5 nm have been previously detected in silicalite-1 by n-hexane porosimetry.[37]

The measured intrinsic zeolite pore size of 0.33 nm is smaller than the size of hydrated ions, for example the hydrated diameter of Na^+ is 0.716 nm, the hydrated diameter of K^+ is 0.662 nm, and the hydrated diameter of Ca^{2+} is 0.824 nm, but the measured pore size is larger than the kinetic diameter of water, 0.276 nm.[39] These results suggest that it is easier for water molecules, than hydrated ions, to enter and exit the intrinsic silicalite pores. For this reason it is likely that most of the ion adsorption, desorption, and exchange observed due to exposure to solutions (Table 3 and Fig. 1) is occurring in the 1.0–1.2 nm micropores and 2.6–4.2 nm mesopores (Table 5).

The intrinsic pores of 0.33 nm appear to be accessible to N_2 (kinetic diameter 0.364 nm[1] or Lennard Jones interaction diameter 0.318 nm[40]). Fig. 9 compares the change in micropore fraction (as measured by N_2 adsorption t-plot analysis relative to BET total area) with the change in micropore and intrinsic pore

Table 5 Summary of PALS data for the original and SW treated silicalite powders. The average pore sizes have been calculated from the lifetimes. Population standard deviations are in parentheses

	Lifetime (ns)			Intensity (%)			Pore Diameter (nm)		
Sample Name	Tau 3	Tau 4	Tau 5	I3	I4	I5	Small Pore	Micropores	Mesopores
Original	0.98 (0.04)	8.02 (0.15)	42.80 (2.54)	14.29 (1.04)	18.24 (0.34)	8.75 (0.08)	0.33 (0.01)	1.05 (0.01)	2.62 (0.13)
SW1h	0.89 (0.02)	8.88 (0.14)	50.46 (1.10)	13.92 (0.64)	11.17 (0.26)	15.36 (0.13)	0.29 (0.01)	1.10 (0.01)	3.03 (0.06)
SW8h	0.92 (0.04)	8.51 (0.22)	55.53 (3.00)	14.36 (1.14)	13.55 (0.48)	12.26 (0.14)	0.31 (0.01)	1.08 (0.01)	3.35 (0.19)
SW16h	0.87 (0.02)	8.69 (0.13)	56.15 (1.31)	14.44 (0.89)	10.96 (0.24)	13.63 (0.09)	0.29 (0.01)	1.09 (0.01)	3.39 (0.09)
SW32h	0.82 (0.04)	10.48 (0.36)	66.81 (2.25)	16.47 (1.44)	5.31 (0.47)	18.40 (0.28)	0.26 (0.01)	1.20 (0.02)	4.19 (0.19)
SW48h	0.88 (0.03)	10.37 (0.44)	58.46 (1.97)	14.57 (1.13)	6.45 (0.25)	17.14 (0.13)	0.29 (0.01)	1.19 (0.02)	3.54 (0.14)

fraction $(I_3 + I_4)/(I_3 + I_4 + I_5)$ as measured by PALS. The sum $I_3 + I_4 + I_5$ represents the relative total pore concentration, intrinsic pores + micropores + mesopores, measured by PALS. The proportion of micropores from both PALS and N_2 adsorption measurements decreases more than 20% after 1 h exposure to SW. The biggest change to micropore proportions (I_3 and I_4) is due to the intercrystalline micropores. The decrease in their relative concentration (I_4) is shown by PALS (Table 5) after 1 h exposure to SW, and this reduction must account for the reduction in micropore proportion obtained from N_2 adsorption measurements as shown in Fig. 9. It is therefore clear that the majority of ion interaction occurs in the intercrystalline pores, which are present both as micro- and mesopores. This interpretation is made possible because PALS is able to distinguish between size and number of pores as well as between the intrinsic zeolite channels and the micropores.

The combined PALS, N_2 adsorption, and ion adsorption results support the concept diagrams in Fig. 9 which show that initially, up to 1 h exposure to SW, monovalent cations Na^+ and K^+ leave the silicalite and some Mg^{2+} enters, and this is reflected in a sharp decrease in 1 nm micropores as indicated by the isotherm relative height $p/p^0 < 0.2$ (Fig. 8 and 9) and the drop in micropore concentration (I_4 PALS). At 8 h, a sharp uptake in Ca^{2+} occurred in tandem with a rise in the micropore concentration in Table 5 and increase in micropore fraction in Fig. 9. At this time, it appears that the presence of more slowly diffusing divalent Ca^{2+} in the micropores is becoming significant such that the micropores open to accommodate this more preferred ion. After 8 h, the trends in adsorption (Fig. 1) and microporosity (Table 5 and Fig. 9) become less complex. Essentially the material gradually expels remaining monovalent cations, replacing them with divalent cations causing a gradual decrease in micropore fraction. An increase in the average micropore size (τ_4) indicates preferential filling of the smaller micropores in the distribution. In micropores with a size of about 1.2 nm, there is space for two divalent ions across the diameter.

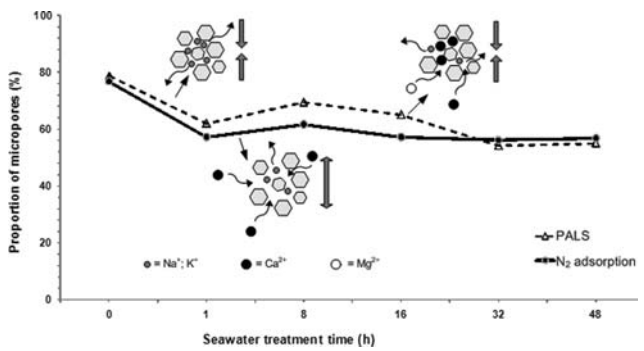

Fig. 9 N_2 adsorption and PALS measurements of changes in micropore proportion of silicalite powders and schematic illustration of these changes caused by ion interactions over SW treatment time.

In our use of PALS together with N_2 adsorption, we found that they both agree well on relative fraction of micropores to total pores (Fig. 9). In our use of these valuable porosimetry techniques, there were differences however in absolute quantities. As PALS is not dependent on external access to the pores,[35] we have utilized it as the measure of all spaces within the zeolite material. According to Fig. 9, both PALS and N_2 adsorption indicate 80% micropores in the original material. However as the micropores begin to fill with ions, external access to micropores for the probing N_2 is restricted, and this restricted access translates to lower micropore fractions observed from the 1 to 16 h samples from N_2 adsorption. The fraction came back to close agreement between PALS and N_2 when these micropores were further filled by ions. The isotherms for the 16 and 32 h exposed samples had higher total uptakes at all relative pressures compared to all other samples. We attribute this again to pore access, because according to PALS (Table 5) these samples have mesopores of large size and concentration which could facilitate more N_2 molecule access to the entire pore structure.

The measurement of an intrinsic pore size of 0.33 nm in our silicalite MFI zeolite compared to the typically observed 0.54–0.56 nm size[11,29,32,36] is attributed to the partial occupancy and replacement behavior of Na^+ ions with K^+ ions in the original silicalite sample. It has been shown[41] that in zeolite NaA (molecular sieve Type 4A), which has an 8-ring opening with diameter of 0.42 nm, partial replacement of Na ions with K ions reduces the pore aperture to 0.3 nm (molecular sieve Type 3A). Modification of zeolite pores for the purpose of molecular sieving has also been achieved by modifying 10-membered ring openings by placing different sized cations in the opening.[42]

The size of the intrinsic zeolite pores decreased from 0.33 nm to 0.29 nm during the first hour of exposure to SW. Helium permeance[37] and water flux[12] also dropped dramatically due to 1 h exposure to water or seawater, respectively. Andersson and Hedlund[37] exposed MFI zeolite to water for 1 day and 30 days and measured the change in mesoporosity and microporosity. Exposure to water alone was shown to reduce the relative permeance of helium through pores <1 nm and increase the relative permeance through the micropores (1–2.5 nm) and mesopores (>2.5 nm). The increase in micropores and mesopores due to

water exposure was attributed to intercrystalline dissolution of synthesis residues and amorphous silica.[37] These results are in complete agreement with our observations of the changes in MFI zeolite porosity on exposure to seawater. The decrease in permeance through the zeolite crystal channels correlates with the decrease in size of intrinsic pores measured here. One possible explanation for the intrinsic pore size reduction observed in this work (from 0.33 nm to 0.29 nm) is the partial exchange of divalent cations for Na^+ and K^+ in the pores. Kuronen *et al.*[43] have shown in zeolite Na-MAX that exchange of K^+ for Na^+ or Sr^{2+} for Na^+ occurs in intrinsic pores that are 0.23 nm diameter that must expand to accommodate the ions. In our work, the ions acted to expand the crystal lattice when exposed (Fig. 6), particularly when K^+ entered the pores from the K^+ rich solutions. As we have focused on realistic seawater concentrations (3.8 wt% TDS), we observed a smaller change in the crystal dimensions (<0.1%) which must be responsible for the slight reduction observed by PALS.

Sorenson *et al.*[44] recently reported volume expansion of the silicalite-1 crystal unit cell (0.5 to 1.5%) due to adsorption of n-alkanes. The Lennard Jones segment diameter of n-alkanes ranges from 0.4524 nm for n-hexane to 0.5233 nm for n-decane,[45] such that these molecules access the 0.55 nm intrinsic silicalite-1 pores. They observed a decrease in flux through intercrystalline defects and attributed the flux decline to the lattice expansion, effectively closing intercrystalline defects. They postulate that the packing of the intrinsic zeolite pores with n-alkanes causes the lattice expansion and also a reduction in intercrystalline micropores. In the present work, because we are able to follow individually the size and concentration of intrinsic pores, micropores and mesopores using PALS, we observe that the slight lattice volume expansion is accompanied by a decrease in intrinsic pore size (which indicates exchange of Na^+ and K^+ in the pores with divalent cations), an overall decrease in micropore concentration (attributed to divalent cation uptake), but an increase in micropore size, mesopore size, and mesopore concentration (attributed to intercrystalline dissolution). We have been able to postulate reasonable explanations for these changes in porosity due to exposure to SW. The development of a fundamental understanding of changes in porosity is essential to controlling the diffusion properties of small molecules and ions through zeolite membranes.

Although defect free zeolite membranes are necessary for excellent salt rejection; preparation of defect free thin films is difficult.[46] In this work we have examined zeolite powders to determine how the intracrystalline and intercrystalline porosity change due to exposure to water and ions. Intracrystalline porosity is characteristic of defect free films and hence the results that relate to the intracrystalline porosity are directly applicable to defect free membranes. We observed an expansion in the crystal dimensions and a reduction in zeolite intrinsic pore size and attributed this to ion exchange.

Intercrystalline porosity is also of interest in that it is highly likely to be present in all membranes and can even be beneficial to flux without compromising salt rejection as long as there are no continuous defect pathways through the thickness of the membrane. We observed that monovalent and divalent cations appear to fill the micropores, and we postulate that this change, perhaps in concert with dissolution in the intercrystalline structure also causes the increase in size and number of the mesopores. Previous studies have reported desalination trials on silicalite membranes[7,12] showing a decrease in water flux, stabilising after about 40 h. Rejection was high for the same ions studied here (60 to 90% rejection) but took over 125 h to stabilise from initially lower values (0 to 40%).[7] From the present work, we can suggest that the gradual increase in divalent ions preferentially occupying the intercrystalline spaces decreases water diffusion but also blocks transport of other ions. The mesopores in the present work would however be expected to contribute to decreasing rejection and increasing flux with time, but we propose that these pores may not be present in membrane films or not continuously connected through the membrane. Although we believe the latter is most likely, analysis of the formed membrane films is needed in future work.

Conclusions

Zeolite-based membranes are novel functional materials for water treatment and potentially offer high tolerance to a variety of realistic feed waters and harsh cleaning methods. In this work, MFI zeolite powders were investigated for their potential use in membranes for seawater desalination which could be accomplished by both pervaporation and RO processes. Studies of ion interactions showed that the prepared silicalite interacts with ions and water when exposed to different solutions (3.8 wt% (TDS) SW, or 1 M NaCl, or 0.05 M KCl). These ion interactions will dictate how the silicalite will perform as desalination membranes either in direct reverse osmosis, or in unique diffusion membranes. The data obtained from synchrotron X-ray powder diffraction, N_2 adsorption, and PALS have indicated that these water and ion interactions result in changes in structure of the zeolites which could have a major impact on their diffusion properties.

Acknowledgements

The financial support provided by the Australian Research Council (ARC) through a Discovery Project (DP0986192) is gratefully acknowledged. This research was undertaken on the Powder Diffraction beamline at the Australian Synchrotron, Victoria, Australia. The authors would like to thank Dr Matthew Hill and Dr Danielle Kennedy of CSIRO, Australia; Dr Kia Wallwork (Australian Synchrotron); Dr Marlene Cran, Dr Nicholas Milne and Noel Dow at Institute for Sustainability and Innovation, Victoria University, Australia; and Yi Huang (Monash University, Australia) for their assistance in sample analysis. Prof Michael Tsapatsis (University of Minnesota, USA) is acknowledged for helpful discussions.

References

1 D. W. Breck, *Zeolite Molecular Sieves - Structure, Chemistry, and Use*, Wiley, New York, 1974.
2 J. Caro and M. Noack, *Microporous Mesoporous Mater.*, 2008, **115**, 215–233.
3 E. E. McLeary, J. C. Jansen and F. Kapteijn, *Microporous Mesoporous Mater.*, 2006, **90**, 198–220.
4 Q. Liu, R. D. Noble, J. L. Falconer and H. H. Funke, *J. Membr. Sci.*, 1996, **117**, 163–174.
5 K. Kusakabe, T. Kuroda and S. Morooka, *J. Membr. Sci.*, 1998, **148**, 13–23.

6 J. H. Dong, Y. S. Lin and W. Liu, *AIChE J.*, 2000, **46**, 1957–1966.
7 L. X. Li, J. H. Dong, T. M. Nenoff and R. Lee, *J. Membr. Sci.*, 2004, **243**, 401–404.
8 J. Lin and S. Murad, *Mol. Phys.*, 2001, **99**, 1175–1181.
9 S. Murad, K. Oder and J. Lin, *Mol. Phys.*, 1998, **95**, 401–408.
10 L. X. Li, J. H. Dong, T. M. Nenoff and R. Lee, *Desalination*, 2004, **170**, 309–316.
11 L. X. Li, J. H. Dong and T. M. Nenoff, *Sep. Purif. Technol.*, 2007, **53**, 42–48.
12 M. Duke, J. O'Brien-Abraham, N. Milne, B. Zhu, Y. S. Lin and J. C. Diniz da Costa, *Sep. Purif. Technol.*, 2009, **68**, 343–350.
13 M. Kazemimoghadam and T. Mohammadi, *Desalination*, 2007, **206**, 547–553.
14 M. Noack, P. Kölsch, A. Dittmar, M. Stöhr, G. Georgi, M. Schneider, U. Dingerdissen, A. Feldhoff and J. Caro, *Microporous Mesoporous Mater.*, 2007, **102**, 1–20.
15 M. Noack, M. Schneider, A. Dittmar, G. Georgi and J. Caro, *Microporous Mesoporous Mater.*, 2009, **117**, 10–21.
16 X. Lin, J. L. Falconer and R. D. Noble, *Chem. Mater.*, 1998, **10**, 3716–3723.
17 U. Illgen, R. Schäfer, M. Noack, P. Kölsch, A. Kühnle and J. Caro, *Catal. Commun.*, 2001, **2**, 339–345.
18 D. S. Bhange and V. Ramaswamy, *Mater. Res. Bull.*, 2006, **41**, 1392–1402.
19 M. Lassinantti Gualtieri, A. F. Gualtieri and J. Hedlund, *Microporous Mesoporous Mater.*, 2006, **89**, 1–8.
20 M. Lassinantti Gualtieri, C. Andersson, F. Jareman, J. Hedlund, A. F. Gualtieri, M. Leoni and C. Meneghini, *J. Membr. Sci.*, 2007, **290**, 95–104.
21 B. F. Mentzen and F. Lefebvre, *Mater. Res. Bull.*, 1997, **32**, 813–820.
22 C. J. Gump, R. D. Noble and J. L. Falconer, *Ind. Eng. Chem. Res.*, 1999, **38**, 2775–2781.
23 H. Morell, K. Angermund, A. R. Lewis, D. H. Brouwer, C. A. Fyfe and H. Gies, *Chem. Mater.*, 2002, **14**, 2192–2198.
24 S. J. Tao, *J. Chem. Phys.*, 1972, **56**, 5499–5510.
25 M. Eldrup, D. Lightbody and J. N. Sherwood, *Chem. Phys.*, 1981, **63**, 51–58.
26 T. L. Dull, W. E. Frieze, D. W. Gidley, J. N. Sun and A. F. Yee, *J. Phys. Chem. B*, 2001, **105**, 4657–4662.
27 G. Bellussi and V. Fattore, in *Zeolite Chemistry and Catalysis (Studies in Surface Science and Catalysis)*, ed. L. Kubelková, B. Wichterlová, P. A. Jacobs and N. I. Jaeger, Elsevier, Amsterdam, 1991, p. 82.
28 B. Kalita and A. K. Talukdar, *Mater. Res. Bull.*, 2009, **44**, 254–258.
29 International Zeolite Association "Database of zeolite structures", http://www.iza-structure.org/databases/, accessed October 2009.
30 K. S. W. Sing, D. H. Everett, R. A. W. Haul, L. Moscou, R. A. Pierotti, J. Rouquerol and T. Siemieniewska, *Pure Appl. Chem.*, 1985, **57**, 603–619.
31 H. Wang, Z. Wang, L. Huang, A. Mitra, B. Holmberg and Y. Yan, *J. Mater. Chem.*, 2001, **11**, 2307–2310.
32 C. A. Cooper and Y. S. Lin, *J. Mater. Sci.*, 2007, **42**, 320–327.
33 H. Li, Y. Sakamoto, Z. Liu, T. Ohsuna, O. Terasaki, M. Thommes and S. Che, *Microporous Mesoporous Mater.*, 2007, **106**, 174–179.
34 A. Mosca, O. Öhrman, J. Hedlund, I. Perdana and D. Creaser, *Microporous Mesoporous Mater.*, 2009, **120**, 195–205.
35 M. C. Duke, S. J. Pas, A. J. Hill, Y. S. Lin and J. C. Diniz da Costa, *Adv. Funct. Mater.*, 2008, **18**, 3818–3826.
36 J. Li, J. Sun, Z. Li, H. Peng, D. Gidley, R. E. Todd and Y. Yan, *J. Phys. Chem. B*, 2004, **108**, 11689–11692.
37 C. Andersson and J. Hedlund, *J. Membr. Sci.*, 2008, **313**, 120–126.
38 A. Cabral-Prieto, I. García-Sosa, J. Jiménez-Becerril, M. Solache-Ríos and S. Bulbulian, *Microporous Mesoporous Mater.*, 2004, **69**, 109–118.
39 E. R. Nightingale Jr., *J. Phys. Chem.*, 1959, **63**, 1381–1387.
40 B. Peng and Y.-X. Yu, *Langmuir*, 2008, **24**, 12431–12439.
41 V. K. Kaushik, R. P. Vijayalakshmi, N. V. Choudary and S. G. T. Bhat, *Microporous Mesoporous Mater.*, 2002, **51**, 139–144.
42 T. Masuda, N. Fukumoto, M. Kitamura, S. R. Mukai, K. Hashimoto, T. Tanaka and T. Funabiki, *Microporous Mesoporous Mater.*, 2001, **48**, 239–245.
43 M. Kuronen, M. Weller, R. Townsend and R. Harjula, *React. Funct. Polym.*, 2006, **66**, 1350–1361.
44 S. G. Sorenson, J. R. Smyth, R. D. Noble and J. L. Flaconer, *Ind. Eng. Chem. Res.*, 2009, **48**, 10021–10024.
45 Y.-X. Yu and G.-H. Gao, *Int. J. Thermophys.*, 2000, **21**, 57–70.
46 J. Choi, H.-K. Jeong, M. A. Snyder, J. A. Stoeger, R. I. Masel and M. Tsapatsis, *Science*, 2009, **325**, 590–593.